Trigonal-Bipyramidal Lewis Base Adducts of Methyltrioxorhenium(VII) and Their Bisperoxo Congeners: Characterization, Application in Catalytic Epoxidation, and Density Functional Mechanistic Study

Fritz E. Kühn,*[a] Ana M. Santos,[a] Peter W. Roesky,[c] Eberhardt Herdtweck,[a] Wolfgang Scherer,[a] Philip Gisdakis,[b] Ilya V. Yudanov,[b, d] Cristiana Di Valentin,[b, e] and Notker Rösch*[b]

Abstract: Methyltrioxorhenium(VII) (MTO) forms trigonal-bipyramidal adducts with pyridines and related Lewis bases. These complexes have been isolated and fully characterized, and two single-crystal X-ray structures are reported. The complexes react with H_2O_2 to form mono- and bisperoxo complexes which were examined in situ by ^1H and ^{17}O NMR spectroscopy. A clear increase in electron deficiency at the Re center can be observed from the MTO complexes to the bisperoxo complexes in all cases examined. The activity of the bisperoxo complexes in olefin epoxidation depends on the Lewis bases, the redox stability of the ligands, and the excess of Lewis base used. Density functional calculations show that when the ligand is pyridine or pyrazole there are significantly stabilized intermediates and moderate energies of the transition states in olefin epoxidation. This ultimately causes an acceleration of the epoxidation reaction. In contrast, the catalytic performance is reduced when the ligand was a nonaromatic nitrogen base. The frontier orbital interaction between the olefin HOMO $\pi(C-C)$ and orbitals with $\sigma^*(O-O)$ character in the LUMO group of the Re-peroxo moiety controls the olefin epoxidation.

Keywords: density functional calculations · epoxidation · peroxo complexes · rhenium · transition states

Introduction

Industrial transformations of olefins into epoxides involve catalysts associated either with hydrogen peroxide, organic peroxides, or oxygen. For the oxidation of fine chemicals, however, stoichiometric reactions are still commonly used.[1] An important improvement in this particular field arose with the discovery by Herrmann and co-workers[2] that methyltrioxorhenium (MTO) and its derivatives act as efficient catalysts for olefin epoxidation. One of the catalytically active species, a bisperoxo complex, was isolated and fully characterized.[3] Since then a broad variety of substituted olefins has been successfully used as substrates[4] and the reaction mechanism has been studied theoretically.[5] The most important drawback of the MTO-catalyzed process is the concomitant formation of diols instead of the desired epoxides, especially in the case of more sensitive substrates.[6] It was quickly detected that the use of Lewis base adducts of MTO significantly decreases the formation of diols as a consequence of the reduced Lewis acidity of the catalyst system. However, while the selectivity increases, the conversion decreases.[6] Use of the urea/H_2O_2 complex instead of aqueous hydrogen peroxide marks another attempt to overcome the formation of diols.[7, 8] Subsequently, it was found that biphasic systems (aqueous phase/organic phase) and addition of a significant excess of pyridine as the Lewis base not only hamper the formation of diols but also increase the reaction velocity in comparison to MTO as the catalyst precursor.[9–11] Recently, it was shown that 3-cyanopyridine and especially pyrazole as Lewis bases are even more effective and less problematic than pyridine itself,[12, 13] while pyridine

[a] Dr. F. E. Kühn, Dipl. Ing. A. M. Santos, Dr. E. Herdtweck, Dr. W. Scherer
Anorganisch-chemisches Institut
der Technischen Universität München
Lichtenbergstrasse 4, D-85747 Garching bei München (Germany)
Fax: (+49) 89-289-13473
E-mail: fritz.kuehn@ch.tum.de

[b] Prof. Dr. N. Rösch, Dipl.-Chem. P. Gisdakis, Dr. I. V. Yudanov, Dipl.-Chem. C. Di Valentin
Institut für Physikalische und Theoretische Chemie
Technische Universität München
Lichtenbergstrasse 4, D-85747 Garching bei München (Germany)
Fax: (+49) 89-289-13622
E-mail: roesch@ch.tum.de

[c] Dr. P. W. Roesky
Institut für Anorganische Chemie der Universität Karlsruhe
Engesserstraße Geb. 30.45, D-76128 Karlsruhe (Germany)

[d] On leave from the Boreskov Institute of Catalysis, Siberian Branch of Russian Academy of Sciences
630090 Novosibirsk (Russia)

[e] Permanent address: Dipartimento di Chimica Organica, Università degli Studi di Pavia
V. le Taramelli 10, I-27100 Pavia (Italy)

 © WILEY-VCH Verlag GmbH, D-69451 Weinheim, 1999 0947-6539/99/0512-3603 $ 17.50+.50/0

N-oxides are less efficient.[14, 15] From in situ measurements under one-phase conditions it was concluded that both electronic and steric factors of the aromatic Lewis base involved play a prominent role during the formation of the catalytically active species. The Brønsted basicity of pyridines lowers the activity of hydronium ions, thus reducing the rate of opening of the epoxide ring.[16] The electronic structure of MTO and its technetium analogue CH_3TcO_3 as well as that of the corresponding trigonal-bipyramidal NH_3 adducts were targets of detailed DF studies.[17]

Despite numerous experimental studies on the effects of pyridine bases on the MTO-catalyzed olefin epoxidation, no MTO-pyridine adduct has yet been fully characterized or even isolated. In this work, we present the characterization of several such complexes, including two single-crystal X-ray structures. Based on these results, we compare in situ examinations with examinations of isolated complexes in catalysis and we present density functional calculations of the epoxidation transition states of bisperoxo complexes as well as a simple orbital interaction model which permits an interpretation of these experimental and computational results. Furthermore, we choose to examine only complexes with pyridines substituted in the *p*-position in order to minimize the steric influence of the Lewis base on the adducts.

Results and Discussion

Synthesis: Several *N*-base adducts of MTO, mainly with aliphatic Lewis bases, have already been reported.[6, 9, 18–22] The scant data on pyridine adducts of MTO which are to be found in the literature have to be regarded with caution because it seems that, according to the ^{17}O NMR and IR data presented,[19, 22] the isolated products are at least partially decomposed to perrhenates.

We will consider several rhenium(VII) complexes in our investigations: MTO (**1**), its monoperoxo complex $[(CH_3)Re(O_2)O_2]$ (**2**), and bisperoxo complex $[(CH_3)Re(O_2)_2O]$ (**3**). The latter compound was also characterized as a water-stabilized complex $[(CH_3)Re(O_2)_2O]\cdot H_2O$[3] (**3′**). The Lewis base adducts under investigation are indicated by a lower case letter, for example, $[CH_3ReO_3]\cdot$py is denoted as **1a**.

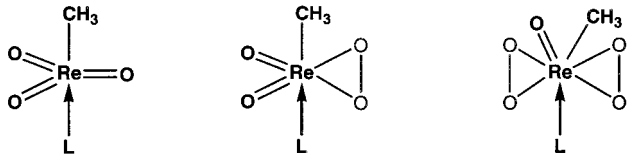

1 **2** **3**

The reaction of MTO with various *p*-substituted pyridines in diethyl ether affords 1:1 adducts of the composition $[CH_3ReO_3]\cdot L$ where L = pyridine (py) (**1a**), 4-methylpyridine (**1b**), 4-*tert*-butylpyridine (**1c**), 4-cyanopyridine (**1d**), and pyridine-4-aldehyde (**1e**) (Scheme 1). The bimetallic complexes $[CH_3ReO_3]_2\cdot L$, where L = 4,4′-bipyridine (4,4′-bipy) (**1f**) and $(NC_5H_4\text{-}CH_2)_2$ (**1g**) are generated by the reaction of 4,4′-bipy or $(NC_5H_4\text{-}CH_2)_2$, respectively, with two equivalents of complex **1**. The pyrazole adduct of MTO (**1h**) has been examined for comparison. In order to isolate the compounds **1a**–**h** the reaction mixture was concentrated and cooled to −78 °C, then a yellow or white precipitate was isolated. Removal of the solvent at room temperature can lead to complete decomposition via red intermediates. The formation of red-colored compounds during the decomposition of Lewis base adducts of organorhenium(VII) oxides has also been observed in the case of aliphatic *N*-bases[23] and might be caused by carbene intermediates (from the deprotonation of the α-C atom of the Re^{VII} center[23, 24]). The final product of the decomposition is dark violet or black and insoluble in all common organic solvents; it seems to consist mainly of ReO_3 (according to IR and elementary analysis). Despite clear evidence that the addition of pyridine stabilizes the peroxo complexes of MTO,[16] the pyridine adduct of MTO is considerably less stable towards moisture and temperature than MTO itself.[23] This enhanced sensitivity has also been observed for other *N*-base adducts of MTO.[23] The complexes **1a**,**b**,**d**,**e**,**h** can be stored under dry inert gases for several weeks at −30 °C; complexes **1c**,**d**,**f**,**g** are stable at room temperature for several days. All complexes react slowly with moisture in the air to give pyridinium perrhenate.

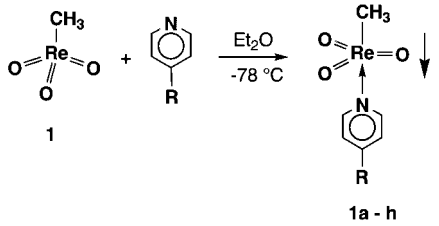

1 **1a - h**

Scheme 1. Synthesis of complexes **1a**–**h**.

Abstract in German: *Methyltrioxorhenium(VII) (MTO) bildet trigonal-bipyramidale Addukte mit Pyridinen und verwandten Lewisbasen. Derartige Verbindungen wurden dargestellt und vollständig charakterisiert, in zwei Fällen auch durch Einkristall-Röntgenstrukturanalyse. Die Komplexe reagieren mit Wasserstoffperoxid unter Bildung von Mono- und Bisperoxokomplexen, welche mit in situ ^{17}O-NMR Spektroskopie untersucht wurden. In allen untersuchten Fällen steigt das Elekronendefizit am Re^{VII}-Zentrum von den MTO-Ligand- zu den Bisperoxokomplexen. Die Aktivität der Bisperoxokomplexe bei der Olefin-Epoxidierung hängt von den Lewisbasen, der Redox-Stabiltät der Liganden und dem Überschuß der eingesetzten Lewisbase ab. Dichtefunktionalrechnungen zeigen, daß Pyridin- und Pyrimidin-Liganden zu deutlich stabilisierten Zwischenprodukten mit moderaten Reaktionsbarrieren für die Olefin-Epoxidierung führen. Letztlich führen sie zu einer Beschleunigung der Reaktion. Nichtaromatische Stickstoffbasen als Liganden verringern die katalytische Aktivität. Die Grenzorbital-Wechselwirkung zwischen dem Olefin-HOMO und den Orbitalen mit σ*(O–O)-Charakter in der LUMO-Gruppe der Rhenium-Peroxo-Einheit kontrolliert die Olefin-Epoxidierung.*

 © WILEY-VCH Verlag GmbH, D-69451 Weinheim, 1999 0947-6539/99/0512-3604 $ 17.50+.50/0 *Chem. Eur. J.* **1999**, *5*, No. 12

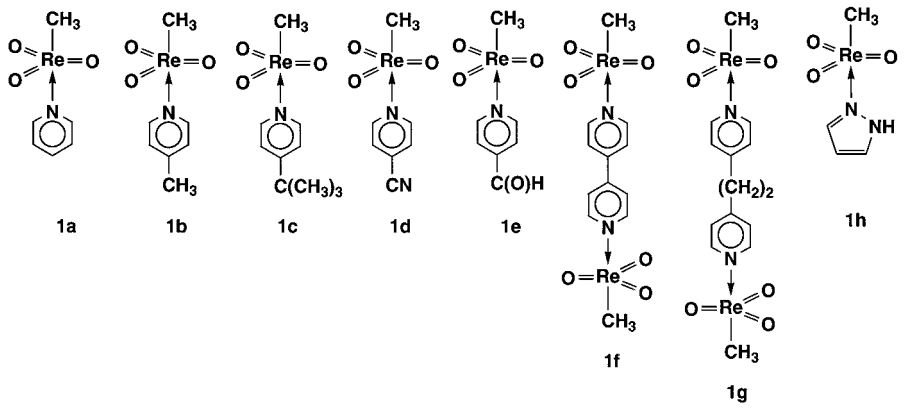

Spectroscopy: IR spectra (recorded in KBr) as well as ^{1}H, $^{13}C\{^{1}H\}$, and ^{17}O NMR spectra (recorded in $CDCl_3$) of the monometallic complexes **1a–e** clearly reflect the decreasing electron-donating capabilities of the ligands in the order **1b** > **1c** > **1a** > **1e** > **1d** (Table 1). This series is in good agreement

Table 1. Selected IR (in KBr), ^{1}H NMR and ^{17}O NMR (in $CDCl_3$) data, and calculated force constants *f*(ReO) for complexes **1**, **1a–h**

Compound	ν(Re=O) [cm^{-1}]	δ(^{1}H)	δ(^{13}C)	δ(^{17}O)	*f*(ReO) [mdyn Å^{-1}]
1	1005 s, 958 vs	2.67	19.03	829	8.53
1a	934 s, 923 vs	1.90	24.91	856	7.43
1b	928 s, 920 vs	1.79	25.43	864	7.36
1c	929 s, 921 vs	1.80	25.15	868	7.38
1d	943 s, 931 vs	2.15	23.28	836	7.58
1e	939 s, 928 vs	2.06	23.80	841	7.52
1f	940 s, 928 vs	2.20	23.26	863	7.53
1g	939 s, 926 vs	1.86	24.27	887	7.49
1h	970 s, 940 vs	2.18	24.62	832	7.84

with the published pK_a values of pyridine derivatives. In this context it is especially noteworthy that the pK_a value of 4-picoline (6.05) is higher than that of 4-*tert*-butylpyridine (5.99), while pyridine has a pK_a value of 5.23.[25] The vibrational frequencies $\tilde{\nu}$(Re=O) of the complexes [$RReO_3$] and [$RReO_3$]·L have been shown to be good indicators for the Re=O bond strength.[26] The corresponding force constants *f*(ReO) can be derived from the ν(Re=O) values (see Table 1).[27] The strongest Lewis bases exhibit the weakest ReO force constants thus indicating that additional electron density donated from the ligand to the Re^{VII} center significantly weakens the Re–O bonds. It has been argued that the formally 14 e system MTO should be regarded as an 18 e system with three ReO bonds of order 2⅔.[28] If additional electron density is introduced into the system, for example by a base ligand, the ReO bond order is reduced and less electron density is withdrawn from the terminal oxygen ligands. This is supported by the ^{17}O NMR spectra of the synthesized complexes (Table 1). The weaker the donor capability of the Lewis base, the closer is, in general, the observed δ(^{17}O) value to that of free MTO (see Table 1). The ^{13}C NMR data are also in good agreement with the IR, ^{1}H, and ^{17}O NMR data: of all the monodentate pyridine adducts examined, **1d** has the closest resemblance to MTO, while **1b** displays the signal with the most prominent shift difference to MTO (see Table 1). This shift difference probably indicates a weakening of the Re–C bond, which may be responsible for the enhanced sensitivity of MTO-pyridine adducts. These complexes usually form pyridinium perrhenates and methanol during hydrolysis. This decomposition pathway provides clear evidence for a weakened Re–C bond. Unfortunately, bond length changes from DF calculations, albeit in the correct direction, are too small to allow a convincing rationalization. In the case of the peroxo complexes, the Re–C bond is strengthened because, in comparison to the terminal oxo groups, peroxo ligands are only weakly donating and therefore less sensitive to hydrolysis. The decomposition pathways of MTO and its peroxo complexes have already been examined in detail.[29] As can be deduced from the spectroscopic data (Table 1), the Lewis base ligand of the bimetallic complex **1g** is a slightly stronger donor than that of **1f**. Furthermore, pyrazole (pK_a = 2.69), is a weaker donor than pyridine (cf. **1a** vs. **1h**; Table 1).

There is also strong support for the fluxonial behavior of the base adducts of type **1** (Scheme 2). If a solution of **1c** in $CDCl_3$ is treated with an equimolar amount of *tert*-butylpyridine *N*-oxide at 35 °C, the original ^{17}O NMR peak at δ = 868

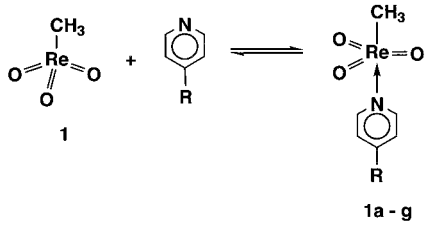

Scheme 2. Dissociation equilibrium which accounts for the fluxonial behavior observed in the ^{17}O NMR spectrum of the base adducts of type **1**.

disappears completely and a new, very broad peak (Δν½ = 1500 Hz) appears at δ = 855. Cooling the solution to −70 °C leads to two signals at δ = 868 and 842 (Δν½ = 800 Hz). The latter peak corresponds to the terminal oxygen ^{17}O NMR signal of the MTO-*tert*-butylpyridine *N*-oxide adduct (**1i**, δ(^{17}O) = 841, Δν½ = 220 Hz). The signals of **1c** and **1i**, *tert*-butylpyridine and *tert*-butylpyridine *N*-oxide can be identified in the ^{1}H NMR spectrum at −70 °C. The signals of **1c** and **1i** exhibit approximately the same size, which indicates a comparable strength of the bond between the base ligand and the Re^{VII} center in both cases. These results also strongly support the ^{1}H NMR data based on calculations of Wang and Espenson who report comparable equilibrium constants for the coordination of pyridine and pyridine *N*-oxide to MTO in CD_3NO_2 at room temperature.[16]

The ^{1}H NMR spectrum of the MTO-pyrazole adduct **1h** shows only three signals for the ligand. The Re center and the

NH proton of the ligand exchange quickly, even at $-70\,^{\circ}C$ in CD_2Cl_2 (Scheme 3). Only broadened signals can be observed; however, the H3 and H5 positions of the pyrazole ligand are still equivalent as a result of the fast exchange process shown in Scheme 3.

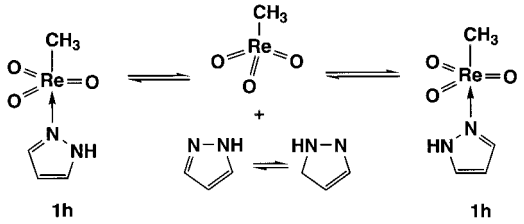

Scheme 3. Fast exchange equilibria in **1h**.

The solid-state structures of **1c** and **1f** are best described as slightly distorted trigonal-bipyramids with the terminal oxygen atoms in the equatorial position (Figures 1 and 2). The oxygen centers are chemically equivalent. The methyl group and the pyridine ligand are *trans* to each other in the apical

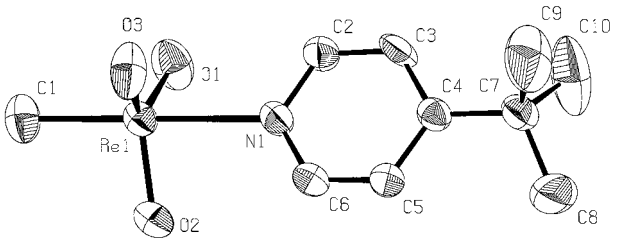

Figure 1. Solid-state structure of **1c** (PLATON drawing; 50% probability ellipsoids; hydrogen atoms omitted for clarity). Selected distances [Å] and angles [°]: Re1–N1 2.407(5), Re1–O1 1.707(4), Re1–O2 1.711(5), Re1–O3 1.705(4), Re1–C1 2.083(7); O1-Re1-N1 83.5(2), O2-Re1-O1 119.3(2), O2-Re1-N1 82.9(2), O3-Re1-N1 83.4(2), O3-Re1-O1 117.6(2), O3-Re1-O2 119.0(2), C1-Re1-N1 179.51(16), C1-Re1-O1 96.1(2), C1-Re1-O2 97.2(3), C1-Re1-O3 97.0(2).

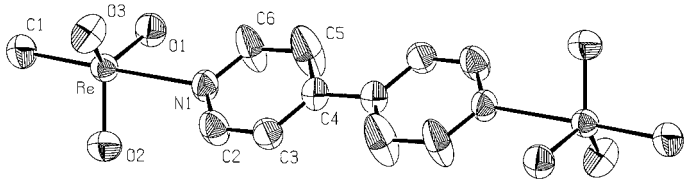

Figure 2. Solid-state structure of **1f** (PLATON drawing; 50% probability ellipsoids; hydrogen atoms omitted for clarity). Selected distances [Å] and angles [°]: Re1–N1 2.504(5), Re1–O1 1.701(5), Re1–O2 1.694(7), Re1–O3 1.695(5), Re1–C1 2.079(7); O1-Re1-N1 80.6(2), O2-Re1-O1 117.6(3), O2-Re1-N1 82.1(2), O3-Re1-N1 81.4(2), O3-Re1-O1 118.3(3), O3-Re1-O2 117.4(3), C1-Re1-N1 178.7(3), C1-Re1-O1 98.2(3), C1-Re1-O2 98.8(3), C1-Re1-O3 98.9(3).

positions. In this coordination the nitrogen lone pair is well stabilized through the interaction with the Re center, while the σ(Re–C) bonding orbital is not affected very much because of the large distance to the two ligands.[17] With respect to the core geometry, **1c** and **1f** resemble the aliphatic base adducts of $[RReO_3]$.[26] In **1c**,**f** the Re–CH_3 bond is slightly elongated in comparison to MTO and the Re=O bond lengths are in all cases equivalent within the range of error. The long Re–N bond lengths indicate a weak interaction of the Lewis base with the Re^{VII} center.[24]

We also carefully checked for any indications that a compound of the composition $[CH_3ReO_3]\cdot py_2$ is formed. However, the reaction of MTO, even with a tenfold excess of pyridine, afforded **1a** as the only isolated product. Furthermore, we did not find any indication in solution that a complex of the composition $[CH_3ReO_3]\cdot py_2$ is present. Further addition of pyridine to a solution of **1a** does not lead to a splitting of the ^{17}O NMR signal, even at $-70\,^{\circ}C$, as would be expected for a $[CH_3ReO_2]\cdot L_2$ complex. If pyridine is used as a solvent, there is still only **1a** present; the resulting chemical shifts in the ^{17}O and ^{1}H NMR spectra are very similar to those recorded in other solvents at very low temperatures. This lack of $[CH_3ReO_3]\cdot py_2$ is probably caused by steric factors. Adducts of the composition $[CH_3ReO_3]\cdot L_2$ are only known for very small Lewis bases, for example NH_3.[18, 19] However, bidentate ligands with a rigid geometry, for example 2,2′-bipyridine, form octahedrally coordinated Lewis base adducts with MTO and related Re^{VII} complexes.[26]

MTO-Lewis base adducts in the presence of H_2O_2: In the presence of excess H_2O_2, MTO is known to react to a bisperoxo complex (**3′**).[4, 5] This reaction proceeds via an intermediate monoperoxo complex (**2**). Compound **2** is also an active catalyst in certain processes.[4, 5, 26] All three complexes—MTO, **2**, and **3′**—are supposed to form pyridine adducts,[16] whereby the pyridine adduct of **3′** is probably the most efficient catalyst by far for the olefin epoxidation. However, the picture is not so clear since the oxidation of pyridine to pyridine *N*-oxide by MTO-peroxo complexes has to be taken into account; furthermore, pyridine *N*-oxide also forms adducts with both MTO and the peroxo complexes.[15] Thus, in recent reports considerable difficulties have been described for attempts to distinguish the different species present only by in situ ^{1}H NMR spectroscopy.[16] We tried to clarify the assignments of the various species observed by performing both ^{1}H and ^{17}O NMR spectroscopy (with ^{17}O-labeled complexes, in order to reduce the measurement times to minutes or less) on all important species in solution. Table 2

Table 2. Selected ^{1}H and ^{17}O NMR data of MTO complexes in $CDCl_3$

Compound	$\delta(^{1}H)$	$\delta(^{17}O)$; $\Delta\nu^{1}/_{2}$[Hz]
MTO (**1**)	2.61	829 (50)
$[(CH_3)Re(O_2)O_2]$ (**2**)	2.90	763 (70)
$[(CH_3)Re(O_2)_2O]\cdot H_2O$ (**3′**)	3.12	753 (180)
MTO·py (**1a**)	1.90	856 (70)
$[(CH_3)Re(O_2)O_2]\cdot$py (**2a**)	2.17	800 (190)
$[(CH_3)Re(O_2)_2O]\cdot$py (**3a**)	2.75	784 (120)
$(MTO)_2\cdot$4,4′-bipy (**1f**)	2.26	863 (190)
$[\{(CH_3)Re(O_2)O_2\}_2]\cdot$4,4′-bipy (**2f**)	2.45	840 (140)
$[\{(CH_3)Re(O_2)_2O\}_2]\cdot$4,4′-bipy (**3f**)	2.79	765 (110)
$(MTO)_2\cdot(NC_5H_4\text{-}CH_2)_2$ (**1g**)	2.06	887 (120)
$[\{(CH_3)Re(O_2)O_2\}_2]\cdot(NC_5H_4\text{-}CH_2)_2$ (**2g**)	2.41	853 (110)
$[\{(CH_3)Re(O_2)_2O\}_2]\cdot(NC_5H_4\text{-}CH_2)_2$ (**3g**)	2.93	783 (160)
MTO·pz (**1h**)	2.19	832 (160)
$[(CH_3)Re(O_2)_2O]\cdot$pz (**3h**)	2.30	755 (100)
MTO·py-*N*-oxide (**1i**)	1.99	847 (100)
$[(CH_3)Re(O_2)O_2]\cdot$py-*N*-oxide (**2i**)	2.33	831 (100)
$[(CH_3)Re(O_2)_2O]\cdot$py-*N*-oxide (**3i**)	2.91	757 (120)

© WILEY-VCH Verlag GmbH, D-69451 Weinheim, 1999
0947-6539/99/0512-3606 $ 17.50+.50/0 *Chem. Eur. J.* **1999**, *5*, No. 12

gives an assignment of the ^1H and ^{17}O NMR spectra of the examined compounds in $CDCl_3$. Isolated compounds were used to identify MTO (**1**) and the bisperoxo complex **3′** as well as their adducts MTO · py (**1a**) and **3a**. In order to detect the monoperoxo rhenium species (pure compound **2** and the corresponding Lewis base adducts **2x**), H_2O_2 was gradually added to the pyridine adducts of MTO to allow the changes in the spectra to be tracked. The pure pyridine *N*-oxide complexes were measured for comparison to facilitate a clear distinction between pyridine and the pyridine *N*-oxide complexes generated by oxidation of pyridine during the measurement processes. We did not observe the formation of a monoperoxo complex **2h** when we started from the pyrazole adduct **1h**. After addition of small amounts of H_2O_2 ($\ll$1 mol equivalent) the signal of complex **1h** was still predominant; a large excess of H_2O_2 led to another signal, which we assigned to the bisperoxo complex **3h**. No ligand oxidation is observed for pyrazole as the Lewis base ligand.

The resulting picture is in good agreement with the expectations. For each ligand, the ^1H NMR signals of the CH_3–Re group are shifted to lower field in the order bisperoxo complex (**3**) > monoperoxo complex (**2**) > MTO complex (**1**). In the ^{17}O NMR spectrum, the terminal oxygen centers of MTO (**1**) and its base adducts **1x** are observed at lower field than in the corresponding peroxo complexes. However, a detailed comparison is problematic in this case for ^{17}O as a nucleus because of the quadrupole moment. The complexes also exhibit significantly different structures that restrict the significance of such a comparison.

Oxidation catalysis: To avoid the presence of a larger amount of the monoperoxo complex (**2**) or its adducts (**2a–h**) during the catalytic reactions, we worked with a large excess of H_2O_2, as is common under catalytic conditions (see the Experimental Section). In our investigations we aimed at clarifying the following questions:

1) Do the different pyridine adducts of MTO exhibit significant differences in their activity which then could be clearly assigned to electronic reasons?
2) Is the catalytic behavior affected if, instead of employing the complexes **1a–h**, we add the base ligands in a "drop in" fashion to the preformed bisperoxo complex **3**?
3) When applying the ligands in considerable excess, are there any additional changes in the catalytic performance, apart from a lower amount of diol formation and a higher reaction velocity?
4) How is the catalytic activity affected by temperature changes?

As substrates we used cyclooctene as the standard olefin and styrene (see below) which is more sensitive to diol formation.

According to the spectroscopic data of the complexes formed and the catalytic results, it does not matter whether the complexes **1a–h** are used as the starting material or whether the ligands are added to the bisperoxo complex **3′** of MTO. Problems can only occur if a long time (days) passes before the second component is added. The base adducts **1a–h** and the MTO-bisperoxo complex **3′** are less stable in solution than the system MTO/py/H_2O_2 (see above).

Lewis base adducts **3x** of the bisperoxo complex **3** form instantaneously in the presence of **1x**; however they do so significantly more slowly when the Lewis base is added to the bisperoxo complex **3′** (as shown by in situ NMR and solution IR spectroscopy). The presence of pyridine *N*-oxide was found to accelerate the formation of MTO peroxo complexes and it was argued[16] that, in view of the mechanism of monoperoxo complex formation, a weakening of the Re=O bond in the starting material would lead to a quicker formation of that monoperoxo complex. Such a bond weakening results from adding Lewis bases to MTO, as can be seen from the changes in the ReO force constants (see above).

The yield of the cyclooctene epoxide is relatively poor if MTO and pyridine bases are used in a 1:1 ratio (Figure 3). In these cases diol formation is only prevented during the first hour of the reaction time. Later on, ring opening of the

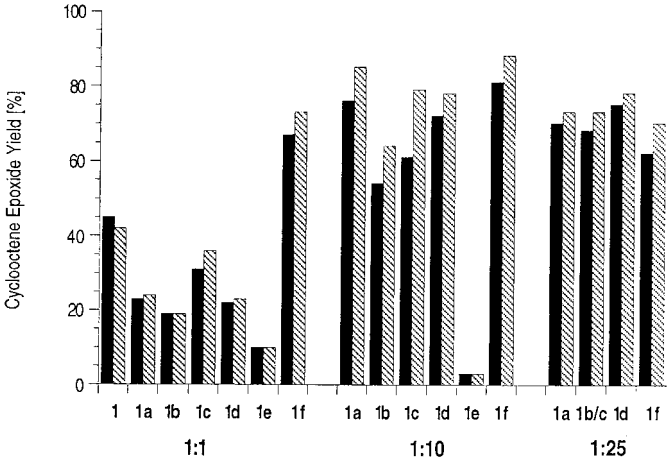

Figure 3. Yields of the cyclooctene epoxidation of MTO–pyridine adducts for various MTO/ligand ratios (1:1, 1:10, and 1:25). All reactions were performed at room temperature with a MTO/H_2O_2/substrate ratio of 0.01:1.5:1. The black bar shows the epoxide yield after 4 h, the hatched bar the yield after 24 h.

primarily formed epoxide occurs, especially in the case of more sensitive olefins, for example cyclohexene[15] or styrene (see below) and under one-phase conditions.[14] Accordingly, even in the case of cyclooctene as a substrate, a prolongation of the reaction time has no positive effect. In some cases more epoxide is transformed to diol during a prolonged reaction time (Figure 3). A tenfold excess of the Lewis base enhances the yield significantly in most cases: the only exceptions are **1e** and **1f**. In the case of **1e**, the Lewis base ligand is oxidized even more easily than cyclooctene. On the other hand, the catalytic performance of **1f** was already very good under "1:1 conditions". (In this particular case, 1 mol of complex forms 2 mol of catalyst; therefore, we worked under the condition 0.5 mol ligand:1 mol MTO.) Interestingly, under 10:1 conditions the best yields are achieved by the use of 4,4′-bipyridine, pyridine, and cyanopyridine. These ligands are not the strongest Lewis bases used. In the case of the 1:1 conditions, the best cyclooctene oxide yields are obtained with *tert*-butylpyridine and 4,4′-bipyridine as ligands, after 4 h. After 24 h the yield was still slowly increasing for all compounds examined (except in the case of pyridine aldehyde); diol

formation was not observed (Figure 3). If a 25-fold excess of Lewis base was used, the product yield changed only marginally relative to the situation with a tenfold excess. However, the yields obtained in the presence of different pyridines are now equal within the range of error. (Under these conditions, the yield with **1b** exactly equals that with **1c** and thus is not separately displayed in Figure 3.) Slight differences in the electron-donor capability of the Lewis bases seem to play only a minor role where there is such a huge excess. Our examinations with pyrazole agree very well with the data of a previous study,[13] corroborating the advantage of this ligand which is not oxidized under the applied conditions. The MTO adduct **3j** of the aliphatic Lewis base quinuclidine, which was measured for comparison, shows a significantly reduced performance in cyclooctene epoxidation when the ligand is used in excess. The strong base quinuclidine promotes the decomposition of MTO (to quinuclidinium perrhenate) in an aqueous system and is a useful ligand for olefin epoxidation only in a "water-free" system, for example in H_2O_2/*tert*-butyl alcohol.[6]

Figure 4 compares the product yields of selected catalysts under 10:1 conditions with styrene as the substrate under two-phase conditions, during the first three hours of reaction time. Aromatic N-donors have an accelerating effect; pyrazole and 4,4′-bipyridine even more than pyridine. The quinuclidine adduct of MTO is not active (no conversion is observed!) in the epoxidation of styrene under these conditions (tenfold excess of ligand, two-phase system H_2O/CH_2Cl_2). This observation will be rationalized below in the discussion of our theoretical studies.

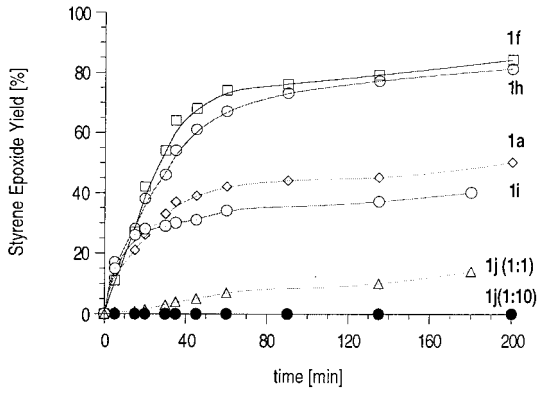

Figure 4. Epoxidation of styrene with different catalyst systems (MTO:ligand = 1:10) in a two-phase system at room temperature. The yields have been determined by GC-MS, after measuring the calibration curves for styrene and styrene epoxide.

Two additional sets of experiments were performed. In contrast to purely inorganic catalysts, a limit for increasing the product yield by increasing the temperature is reached relatively quickly with Lewis base adducts of MTO. Already at 55 °C the total yield after 4 h is significantly lower than at room temperature in all cases examined, regardless of the excess ligand used. The yields at 0 °C, however, are approximately equal to the yields at room temperature. This is an important result, considering that the ligand–Re^{VII} interaction is considerably weakened at higher temperatures.[20] Catalysis with chiral Lewis bases as auxiliaries should be much more successful if the reaction temperature is kept low. Therefore, it is important to know which effects on the yield are to be expected under such conditions. As the activity of the oxidation solutions remains unchanged when cooled down to room temperature after a high temperature run at 55 °C and reused, the lower yield at higher reaction temperatures is not caused by catalyst decomposition, at least not to a significant extent. The influence of the weakly coordinating ligand is reduced because of the temperature influence on the equilibrium shown in Scheme 2.

Theoretical investigations: In a recent DF study[5] we showed that olefin epoxidation catalyzed by MTO mainly takes place by a "front" side (opposite to the methyl ligand) spiro attack of the olefin at a peroxo group of a bisperoxo complex. A base ligand coordinated at the Re center was calculated to stabilize bisperoxo complexes thermodynamically; however, it was also found to significantly change the electronic structure of the complex to lead to a decrease in its reactivity. Oxygen-transfer reactions involving d^0 transition metal peroxo species are assumed to proceed through an attack of the electrophilic oxygen center, as shown for the sulfoxidation of thianthrene 5-oxide by V, Mo, and W peroxo complexes.[30] The epoxidation activity of the peroxo group in the complex is mainly controlled by three factors:[31]

1) the strength of the M–O and O–O interactions which are, to some extent, reflected by the corresponding bond lengths (these bonds are to be broken during the reaction),
2) the charges on the peroxo oxygen centers and the olefin, as a measure of electrophilicity of oxygen and nucleophilicity of olefin, and
3) the interaction between the peroxo σ*(O–O) orbital in the LUMO group of the metal complex and the π(C–C) HOMO of the olefin (Figure 5).

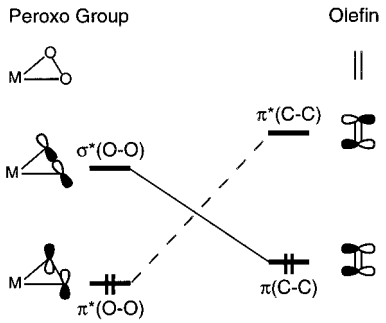

Figure 5. Schematic representation of the frontier orbital interactions between a transition metal peroxo complex and an olefin.

These factors, which are not completely independent of each other, may be invoked to rationalize the effect of a base ligand on the reactivity of the rhenium bisperoxo complex. For this purpose, we chose the base-free complex $[CH_3Re(O_2)_2O]$ (**3**) and carried out calculations on a series of adducts $[CH_3Re(O_2)_2O]\cdot L$ with different bases where L = H_2O (**3′**), pyridine (**3a**), pyrazole (**3h**), pyridine *N*-oxide (**3i**), NH_3 (**3k**), and NMe_3 (**3l**) (Figure 6). The complex **3l** was studied to model the experimentally characterized quinucli-

© WILEY-VCH Verlag GmbH, D-69451 Weinheim, 1999
0947-6539/99/0512-3608 $ 17.50+.50/0 *Chem. Eur. J.* **1999**, *5*, No. 12

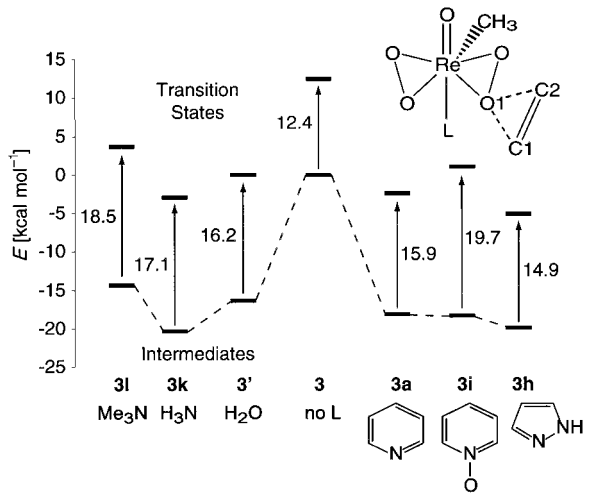

Figure 6. Stabilization energies of various base adducts $[CH_3Re(O_2)_2O]\cdot L$ (**3x**) and the corresponding epoxidation transition states (for a frontal attack of ethylene as a model olefin), relative to the energy of the base-free bisperoxo complex $[CH_3Re(O_2)_2O]$ (**3**).

dine adduct **3j**. $[CH_3Re(O_2)_2O]\cdot NH_3$ (**3k**) was calculated to analyze the effect of a sterically unhindered amino complex; its monoligated precursor complex $[CH_3ReO_3]\cdot NH_3$ is not known; however, the pseudo-octahedral complex $[CH_3ReO_3]\cdot 2NH_3$ has been characterized by elemental analysis, IR, and NMR spectroscopy.[18] We computationally characterized these complexes and their transition states for the epoxidation of ethylene as a model olefin; effects of olefin substitutents were also investigated. We focused on a frontal spiro attack as the energetically most favorable reaction pathway;[5] for the present study, we did not consider other reaction mechanisms, such as an attack of hydroperoxy intermediates which are favored for titanium or molybdenum peroxo complexes.[31]

Bisperoxo complexes: The calculated structural and energetic parameters of compound **3**, the various base adducts $[CH_3Re(O_2)_2O]\cdot L$, and the corresponding transition states for ethylene epoxidation are compiled in Table 3. Figure 6 shows the stabilization of the ligated bisperoxo complexes $[CH_3Re(O_2)_2O]\cdot L$ (**3x**) relative to the base-free compound **3** and the corresponding heights of the energy barrier for ethylene epoxidation. The six base ligands studied theoretically have different interaction energies E(Re–L) with the bisperoxo complex **3**. NH_3 and pyrazole exhibit strong binding, $\approx$20 kcal mol^{-1}, followed by pyridine *N*-oxide and pyridine with very similar interaction energies of $\approx$18 kcal mol^{-1}. H_2O and NMe_3 feature noticeably smaller metal–ligand binding energies, $\approx$16 and 14 kcal mol^{-1}, respectively. Comparison of the structural parameters and the partial charges from a natural population analysis (NBO analysis) of the base adducts with NMe_3 and NH_3 reveals (Table 3) that the reduced metal–ligand binding energy of the former base is caused by steric repulsion between the methyl substituents of the base and other ligands of the Re center. In this case, the Re–N bond length is elongated by $\approx$0.2 Å; however, the charge distribution is quite similar to that calculated for other base adducts.

The coordination of a base ligand to the bisperoxo complex **3** elongates the Re–O1 bonds, which leads to a slight shortening of the O–O peroxo bond (except for pyrazole where the O–O distance remains unchanged). During the epoxidation reaction, the bonds C1–O1 and C2–O1 are

Table 3. Structural and energetic parameters[a] of the complexes $[CH_3Re(O_2)_2O]\cdot L$ and the corresponding transition states of a frontal spiro attack by ethylene as a model olefin.

L	Me_3N **3l**	H_3N **3k**	H_2O **3′**	No base[b] **3**	Pyridine **3a**	Pyridine-*N*-oxide **3i**	Pyrazole **3h**
Intermediate							
d(Re–L)[c] [Å]	2.637	2.431	2.481	–	2.504	2.359	2.415
d(Re–O1) [Å]	1.960	1.963	1.962	1.944	1.960	1.960	1.963
d(O1–O2) [Å]	1.447	1.446	1.449	1.450	1.449	1.447	1.450
q(L) [e]	0.15	0.17	0.11	–	0.14	0.16	0.16
q(Re) [e]	1.95	1.92	1.97	2.05	1.97	1.95	1.92
q(O1) [e]	–0.38	–0.38	–0.39	–0.36	–0.37	–0.40	–0.37
q(O2) [e]	–0.36	–0.35	–0.35	–0.35	–0.37	–0.36	–0.40
σ^*(O1–O2)[d] [eV]	–0.50	–0.47	–0.81	–0.99	–0.36	–0.10	–0.43
Δ(O1 1s)[e] [eV]	0.73	0.75	0.47	0.00	0.94	1.12	0.81
E(Re–L) [kcal mol^{-1}]	–14.4	–20.3	–16.3	–	–18.1	–18.3	–19.8
transition State							
d(C1–O1) [Å]	2.206	2.124	2.117	2.070	2.080	2.005	2.076
d(C2–O1) [Å]	2.040	2.082	2.090	2.206	2.146	2.203	2.116
d(C1–C2) [Å]	1.357	1.358	1.358	1.357	1.358	1.357	1.357
d(Re–O1) [Å]	2.053	2.050	2.052	2.024	2.034	2.023	2.034
d(O1–O2) [Å]	1.826	1.836	1.833	1.798	1.827	1.816	1.820
q(C1) [e]	0.15	0.15	0.15	0.19	0.17	0.19	0.17
q(C2) [e]	0.19	0.19	0.19	0.15	0.17	0.15	0.16
q(C1) + q(C2) [e]	0.34	0.34	0.34	0.34	0.34	0.34	0.33
ΔE [kcal mol^{-1}]	18.5	17.1	16.2	12.4	15.9	19.7	14.9

[a] Bond lengths d, partial charges q from a natural population analysis, formation energy of the base adduct E(Re–L), and energy barrier ΔE of epoxidation. For the atom designations, see Figure 6. [b] Base-free reference complex $[CH_3Re(O_2)_2O]$. [c] Re–N bond length, except for H_2O where Re–O is given. [d] Average energy of virtual orbitals with strong σ^*(O1–O2) character in the LUMO complex of $[CH_3Re(O_2)_2O]\cdot L$. [e] Shift of the O1 1s Kohn–Sham orbital energy relative to the value of the base-free reference complex, –523.227 eV.

formed (Figure 6), while the Re–O1 and the O1–O2 bonds are broken. Thus, the strength of the latter two bonds is expected to influence the barrier height. The bonds Re–O1 and O1–O2 are not independent. Invoking bond order conservation, one expects an elongation of the Re–O bonds of the peroxo group to be accompanied by a shortening of the O–O bond. Therefore, it is not straightforward to predict a correlation between these bond lengths and the height of the reaction barrier. Inspection of Table 3 reveals that, among all base adducts investigated, **3h** features the longest Re–O1 and O1–O2 bond lengths and the smallest energy barrier. On the other hand, **3i** exhibits the shortest Re–O1 bond length and one of the shortest O1–O2 bonds as well as the highest epoxidation barrier.

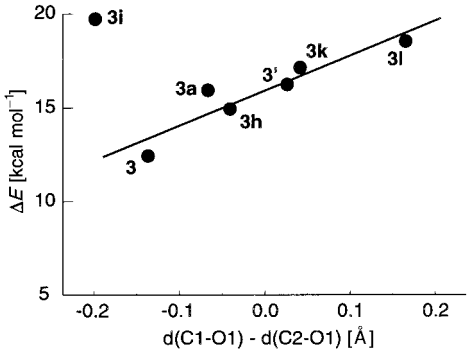

Figure 7. Calculated energy barrier ΔE of ethylene epoxidation as function of the difference of the interatomic distances d(C1–O1) – d(C2–O1) of various base adduct transition states.

Structures of the transition states: As discussed below, the activation of the peroxo bond O1–O2 is mainly controlled by an interaction between the occupied olefin π(C–C) orbital and the unoccupied σ*(O–O) orbital of the metal complex. Therefore, one expects the elongation of the O–O bond in the transition state to be the most significant structural change relative to the base adducts. This is indeed the case: the O–O distance increases by 0.35 Å (**3**) to 0.39 Å (**3k**) (Table 3). On the other hand, all transition states studied exhibit similar values of the C–C bond lengths, ≈1.36 Å, which is only slightly elongated compared to the value calculated for ethylene, 1.327 Å. The calculated C–C bond length of ethylene epoxide is 1.47 Å.

In a combined experimental and computational study it has been concluded[32] that olefin epoxidation with organic peracids features an essentially concerted approach of the olefin to the relevant peroxo oxygen center. The transition states determined in the current work also support such a conclusion for the Re bisperoxo complexes under study. The two bond lengths C1–O1 and C2–O1 in the transition states differ by at most 0.20 Å (for L = pyridine *N*-oxide; Table 3). The olefin carbon atom C1 is the one closer to the base ligand binding site of the Re bisperoxo complex in the transition state, while the carbon atom C2 points in the direction of the oxo group (see Figure 6 for the atom labeling). The position of the shorter C–O bond is not the same for all structures. The base-free complex **3** and the base adducts **3a**, **3i**, and **3h** exhibit a longer C2–O1 bond, while the opposite holds for the complexes **3l**, **3k**, and **3′**. Interestingly, the asymmetry of the transition state structure correlates very well with the barrier height (Figure 7): the shorter the distance d(C2–O1) compared to d(C1–O1), the lower is the barrier. (Only the pyridine *N*-oxide adduct **3i** forms an exception.) This finding suggests that the differences between the two C–O distances in the transition state do not result from steric factors, but are caused by electronic interaction. As expected, the carbon atom closer to the oxygen center is more positively charged (Table 3). With the exception of NMe_3, the difference between the charges of the two carbon centers correlates quite well with the difference between the C–O distances. However, the differences are not large enough (Table 3) to support the hypothesis of an ionic charge distribution, as would be expected for a nonconcerted mechanism. The partial charge of the olefin in the transition state (as measured by q(C1) + q(C2); Table 3) provides an estimate for the amount of electron density donated by the olefin. This transfer of electron density from the olefin to the metal complex is the same for all base ligands.

MO analysis: To rationalize the influence of the charge distribution within the complex on its reactivity, it is useful to consider how the frontier orbitals of the olefin and the peroxo group interact during the reaction. Figure 5 presents the corresponding orbital interaction in a simplified fashion. The dominant interaction occurs between the olefin HOMO π(C–C) and the unoccupied peroxo σ*(O–O) orbital, which is among the LUMO group of the metal peroxo complex. Through this interaction, electron density is redistributed from the C–C bonding olefin orbital to an O–O antibonding orbital, and thus entails O–O bond activation. The reciprocal interaction between the π*(O–O) HOMO of the metal peroxo complex and the olefin LUMO π*(C–C) is less important since the corresponding energy gap is larger (Figure 5).[31] The reactivity of the metal complex depends mostly on the first interaction and thus on the overlap between the two π(C–C) and σ*(O–O) orbitals as well as on the corresponding energy gap.

Alkyl substituents on the olefin raise the π(C–C) level through electron donation; thus, the gap between the frontier orbitals decreases and the epoxidation barrier is expected to decrease accordingly. To corroborate this effect, we have determined the barrier heights of olefin epoxidation for the unligated bisperoxo reference complex $[CH_3Re(O_2)_2O]$ and several of its base adducts $[CH_3Re(O_2)_2O]\cdot L$ (Table 3). Figure 8 displays the calculated energy barriers for the epoxidation of ethylene and its methyl-substituted derivatives via the base-free complex **3** as a function of the olefin π(C–C) orbital energy. We note a substantial lowering of the epoxidation barrier from 12.4 kcal mol^{-1} for ethylene to 6.3 kcal mol^{-1} for tetramethylethylene. The higher energy of the olefin π(C–C) orbital reflects the more nucleophilic nature of the olefin concomitant with a lower activation barrier of the epoxidation reaction. The linear variation of the epoxidation barrier with the olefin HOMO energy underlines the importance of the underlying frontier orbital interaction.

By the same token, one expects a higher epoxidation barrier if the virtual orbitals in the LUMO group of the

 © WILEY-VCH Verlag GmbH, D-69451 Weinheim, 1999 0947-6539/99/0512-3610 $ 17.50+.50/0 *Chem. Eur. J.* **1999**, *5*, No. 12

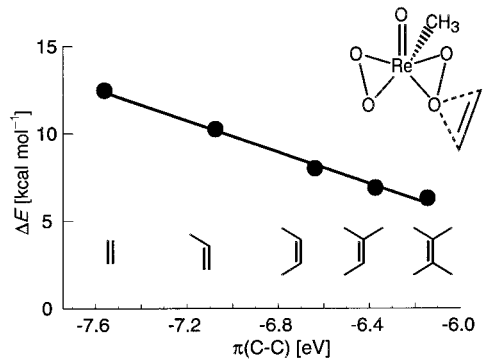

Figure 8. Calculated energy barriers ΔE for epoxidation of various substituted olefins by the base-free reference complex $[CH_3Re(O_2)_2O]$ (**3**) as a function of the energy of the HOMO π(C–C).

M-O-O moiety with significant σ*(O–O) contribution (Figure 5) are raised in energy. Thus, for a given olefin, coordination of a base is expected to increase the relevant HOMO–LUMO gap and thus decrease the dominant frontier orbital interaction with the incoming olefin. All base ligands L transfer electron density to the Re center (see q(Re) in Table 3) and thus reduce its ability to withdraw electron density from the peroxo group. Therefore, the more negatively charged peroxo oxygen centers of the base adducts are less amenable to a nucleophilic attack by an olefin. In Table 3 we present the energy of the σ*(O–O) orbital as well as the shift Δ(O1 1σ) of the 1s core level of the O1 center relative to the value in the base-free complex $[CH_3Re(O_2)_2O]$. Since the systems studied exhibit similar core structures and since changes as a result of rehybridization of the M–O and the O–O bonds are negligible, the oxygen core level energy depends mainly on the local charge density. The core level shift (related to the negative of the ESCA shift) may be taken as a measure of the charge on the O1 center: the more positive the shift, the larger the negative charge on the corresponding center. Figure 9a illustrates how the 1s core level shift varies with the energy of the donating lone pair orbital σ_{lp} of the isolated Lewis base. The purely σ-donating ligands H_2O, NH_3, and pyridine *N*-oxide (with the exception of NMe_3) show a correlation. On the other hand, pyrazole and pyridine, which exhibit an additional π interaction channel with the metal center, do not obey the same relationship; NMe_3 deviates because of significant structural differences (Re–N bond length; see Table 3). We note that the σ*(O–O) level and the 1s core level are shifted synchronously when the base ligand L is varied (see Figure 9b). Both orbitals are localized on the oxygen centers; therefore, they both react similarly to the change in the potential when the electron density is increased as a result of coordination of an electron-donating base ligand at the rhenium center.

Figure 9c shows how the energy of the epoxidation barrier changes with the energy of the σ*(O–O) orbital. Ligands with an additional π-interaction channel feature noticeably lower barriers for the epoxidation reaction. The general trend is indeed as discussed above: a system where the ligand pushes more electron density to the oxygen atom features a higher barrier for epoxidation.

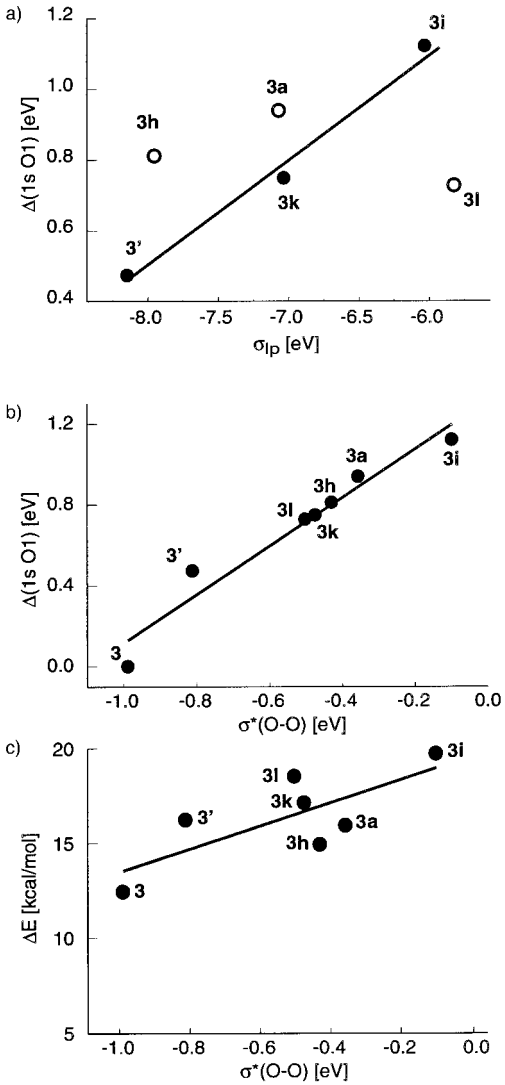

Figure 9. a) Peroxo O1 1s Kohn–Sham orbital energy shift Δ(O1 1s) of various base adducts $[CH_3Re(O_2)_2O]\cdot L$ (**3x**) (calculated relative to the value of the base-free reference complex **3**, –523.227 eV) as a function of the energy of the donating lone-pair level σ_{lp} of the free ligand L. b) Δ(O1 1s) of complexes **3x** as a function of the σ*(O–O) orbital energy. c) Calculated energy barrier ΔE for ethylene epoxidation by various base adducts $[CH_3Re(O_2)_2O]\cdot L$ (**3x**) as a function of the σ*(O–O) orbital energy of **3x**.

A natural population analysis reveals that the base ligands carry a notable positive charge and it reflects the reduction of the positive charge on the metal center just mentioned as a result of the formation of a base adduct. Furthermore, more electron density is found on the peroxo oxygen center O1 which is attacked by the olefin (Table 3). However, the O1 charge values vary over such a narrow range that it is not possible to establish a meaningful correlation with the calculated barrier heights. The charge of the base ligand does not correlate with the charge of the oxygen center O1. A water ligand exhibits the smallest positive ligand charge, yet the Re-peroxo moiety is quite polarized. Pure σ-donor ligands, such as NMe_3, NH_3, H_2O, and pyridine *N*-oxide, support a higher charge on the O1 center than the conjugated N-bases pyridine and pyrazole, which can act both as π-donor and π-acceptor ligands. Inspection of Figure 9c shows that the barrier height

 © WILEY-VCH Verlag GmbH, D-69451 Weinheim, 1999 0947-6539/99/0512-3611 $ 17.50+.50/0

within the group of pure σ-donor ligands (**3l**, **3k**, **3′**, and **3i**) varies quite linearly with the energy of the σ*(O–O) orbital. Because of the correlation displayed in Figure 9b, the calculated barrier height of ethylene epoxidation also correlates with the charge on the O1 oxygen center of the attacked peroxo group. On the other hand, ligands which are also able to interact with the metal center through a π-channel (**3a** - pyridine, **3h** - pyrazole) feature relatively low epoxidation barriers (Figure 4).

It is instructive to correlate the calculated reaction barriers of ethylene epoxidation by various Lewis base adducts **3x** with the corresponding experimental yields of the catalytic epoxidation of styrene. In Figure 10 the yield of styrene oxide with **1a,h–j** as the starting material (after $t = 200$ min) is displayed as function of the calculated energy of the transition

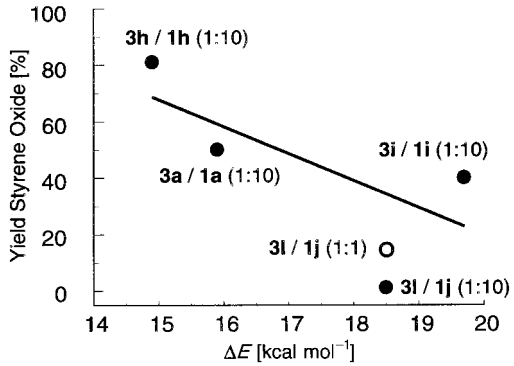

Figure 10. Yields of styrene oxide (after 200 min) as function of the calculated transition state energy ΔE (see Table 3, ethylene as a model olefin). The first label denotes the calculated transition state complex (see Figure 6), the second label the experimental starting material (ratio MTO:Lewis base in parenthesis, see Figure 4).

state of ethylene epoxidation (see ΔE values in Table 3). As discussed above, substitution of the olefin only causes a linear shift of the barrier (see Figure 7). Figure 10 demonstrates the overall effect of a base ligand of complex **3**: the lower the energy of the transition state, the higher the epoxidation yield. System **3l** does not fit the correlation very well. This may be rationalized by the fact that, because of the steric repulsion (cf. d(Re–L) of 2.64 Å and E(Re–L) of 14.4 kcal mol^{-1}, see Table 3), the metal–ligand bond is rather weak. Thus, the ligand may be displaced, for example by a water molecule, and in that case the base adduct is not well defined.

Energetics: The overall effect of the model base ligands on the reactivity of the rhenium peroxo complexes is a combination of stabilization and deactivation of the rhenium bisperoxo base adduct. To evaluate this combined effect, we compared the energetics of each system to that of the base-free complex **3** (Figure 6). Obviously, the base-free system features the lowest activation barrier relative to its precursor intermediate, yet it also exhibits the highest transition state (by absolute energy), since it lacks the stabilization afforded by the base ligand. In general, the stabilization of the intermediate ($\approx$14–20 kcal mol^{-1}) surpasses the increase of the energy barrier to the transition state by far, which ranges from -2.2 kcal mol^{-1} for pyridine to -3.2 kcal mol^{-1} for NH_3, and -4.9 kcal mol^{-1} for pyrazole. However, among the model bases investigated there are also noteworthy exceptions to this trend. The strong stabilization afforded by a water ligand is essentially compensated by a large enhancement of the activation energy. Therefore, **3′** has an epoxidation transition state that lies at a higher energy (by absolute value) than the transition states of **3a** and **3h**. Since water is always present under catalytic conditions, one effect of a base ligand in the catalytic process is quite clear. By ensuring a stronger stabilization than water, a favorable base extrudes the water ligand from the complex; however, at the same time it must not deactivate the complex too much. Pyridine fulfills both these conditions although it can easily be oxidized to pyridine *N*-oxide which provides a similar stabilization but induces a much higher epoxidation barrier. Among the ligands studied, pyrazole affects the catalytic reaction optimally since it affords the largest stabilization of the intermediate and leads to the smallest increase of the activation barrier. On the other hand, the base NMe_3 exhibits the least stabilization of the base adduct and entails a rather strong increase of the activation energy. The calculated reaction barriers correlate quite well with the experimentally determined yields of styrene epoxidation (Figure 10).

Conclusions

In the presence of excess H_2O_2 all the Lewis base adducts of MTO examined form bisperoxo complexes. The reactivity of these complexes varies significantly depending on the Lewis base ligand, despite the fluxonial behavior of these complexes in solution. Ligand stability against oxidation by H_2O_2, excess of the ligand under catalytic conditions, and the reaction temperature all affect the catalytic efficiency. According to our density functional investigations, the coordination of a Lewis base ligand to the rhenium bisperoxo complex generally increases the barrier to olefin epoxidation because the base ligand donates electron density to the peroxo group through the metal center thus reducing its electrophilic properties. The frontier orbital interaction between the olefin HOMO π(C–C) and the orbitals with σ*(O–O) character in the LUMO group of the metal peroxo moiety controls the activation of the O–O bond. The olefin HOMO is pushed to higher energies by electron-donating alkyl substituents, with the epoxidation barrier dropping concomitantly. On the other hand, a base coordinated at the metal center pushes the σ*(O–O) LUMO to higher energies and thus entails a higher barrier for epoxidation. The pyrazole ligand affords the largest stabilization of rhenium bisperoxo complexes, surpassing even water. In addition, pyrazole also features the smallest deactivating effect. As a result, if present at a high enough concentration, a favorable Lewis base (such as pyrazole) is able to expel the water ligand (which induces a higher barrier) from the rhenium center, thus accelerating the olefin epoxidation reaction.

© WILEY-VCH Verlag GmbH, D-69451 Weinheim, 1999
0947-6539/99/0512-3612 $ 17.50+.50/0 *Chem. Eur. J.* **1999**, *5*, No. 12

Experimental Section

All preparations and manipulations were carried out with standard Schlenk techniques under an oxygen-free and water-free nitrogen or argon atmosphere. Solvents were dried by standard procedures, distilled, and kept under argon over 4 Å molecular sieves. Microanalyses and mass spectra were performed at the TUM (Garching) laboratories. IR spectra were measured on a Perkin-Elmer FT-IR spectrometer and mass spectra were obtained with a Finnigan MAT 311 A and a MAT 90 spectrometer. Mass spectra (*m*/*z* values) are based on the isotope ^{187}Re. ^{1}H NMR (399.80 MHz), ^{13}C NMR (100.51 MHz), and ^{17}O NMR (54.14 MHz) spectra were recorded on a JEOL JNM GX-400. The starting compound **1** was prepared according to the literature.[33] The other chemicals were used as purchased or prepared as described below.

Preparation of complexes of general formula (pyridine)methyltrioxorhenium and (pyrazole)methyltrioxorhenium (2): Pyridine (pyrazole) (2.0 mmol) was added to a solution of **1** (250 mg, 1.0 mmol) in diethyl ether (10 mL). The solution turned yellow. The mixture was stirred for 2 h and then concentrated to ≈5 mL. A yellow or nearly colorless precipitate was obtained upon cooling to −78 °C, washed with pentane, and dried in a vacuum (oil pump).

Methyl(pyridine)trioxorhenium (1a): Yield: 150 mg (48 %); IR (KBr): $\tilde{\nu}$ = 3065 w (C=CH), 1603 m (C=C), 1447 s, 934 vs (Re=O), 923 vs (Re=O), 737 s, 699 m, 630 m, 429 m cm^{-1}; ^{1}H NMR (400 MHz, $CDCl_3$, RT): δ = 1.90 ($ReCH_3$, s, 3H), 7.34–7.38 (N(CH)(C*H*), m, 2H), 7.75–7.82 (N(CH)(CH)(C*H*), m, 1H), 8.25–8.27 (N(C*H*), m, 2H); ^{13}C{^{1}H} NMR (100.51 MHz, $CDCl_3$, RT): δ = 24.91 ($ReCH_3$), 125.02 (N(CH)(*C*H)), 138.63 (N(CH)(CH)(*C*H)), 146.86 (N(CH)); CI-MS (70 eV): *m*/*z* (%): 251 (100) [CH_3ReO_3+H$^+$]$^+$, 235 (77) [ReO_3)]$^+$; anal. calcd for $C_6H_8NO_3Re$ (328.34): C 21.95, H 2.46, N 4.27, O 14.62, Re 56.71; found: C 21.94, H 2.47, N 4.26, O 14.58, Re 57.36.

Methyl(4-methylpyridine)trioxorhenium (1b): Yield: 230 mg (67 %); IR (KBr): $\tilde{\nu}$ = 1616 vs (C=C), 1440 m, 1418 m, 928 vs (Re=O), 920 vs (Re=O), 808 s, 562 m, 493 m cm^{-1}; ^{1}H NMR (400 MHz, $CDCl_3$, RT): δ = 1.79 ($ReCH_3$, s, 3H), 2.35 (py-CH_3, s, 3H), 7.16 (N(CH)(C*H*), d, ^{3}J(H,H) = 6.10 Hz, 2H), 8.06 (N(C*H*), d, ^{3}J(H,H) = 4.89 Hz, 2H); ^{13}C{^{1}H} NMR (100.51 MHz, $CDCl_3$, RT): δ = 21.05 (py-CH_3), 25.43 ($ReCH_3$), 125.92 (N(CH)(*C*H)), 146.23 (N(CH)(CH)(*C*H)), 150.92 (N(CH)); CI-MS (70 eV): *m*/*z* (%): 251 (83) [CH_3ReO_3+H$^+$]$^+$, 235 (100) [ReO_3)]$^+$; anal. calcd for $C_7H_{10}NO_3Re$ (342.36): C 24.59, H 2.94, N 4.09, O 14.02, Re 54.39; found: C 24.70, H 2.94, N 4.09, O 13.97, Re 54.50.

(4-*tert*-Butylpyridine)methyltrioxorhenium(VII) (1c): Yield: 200 mg (52 %); IR (KBr): $\tilde{\nu}$ = 2965 m (C-H), 1614 s (C=C), 1419 m, 929 vs (Re=O); 921 vs (Re=O) cm^{-1}; ^{1}H NMR (400 MHz, $CDCl_3$, RT): δ = 1.26 ((CH_3)$_3$C, s, 9H), 1.80 ($ReCH_3$, s, 3H), 7.34 (N(CH)(C*H*), dd, ^{3}J(H,H) = 4.88 Hz, ^{4}J(H,H) = 1.83 Hz, 2H), 8.13 (N(C*H*), dd, ^{3}J(H,H) = 4.88 Hz, ^{4}J(H,H) = 1.83 Hz, 2H); ^{13}C{^{1}H} NMR (100.51 MHz, $CDCl_3$, RT): δ = 25.15 ($ReCH_3$), 30.17 ((CH_3)$_3$C), 35.00 ((CH_3)$_3$*C*), 122.17 (N(CH)(*C*H)), 146.44 (N(CH)(CH)(*C*)), 163.62 (N(*C*H)); CI-MS (70 eV): *m*/*z* (%): 271 (12) [$NC_5H_4(C(CH_3)_3)$)$_2$]$^+$, 235 (5) [ReO_3)]$^+$, 136 (100) [$NC_5H_4(C(CH_3)_3)$)]$^+$; anal. calcd for $C_7H_7N_2O_3Re$ (384.45): C 31.24, H 4.19, N 3.64, Re 48.43; found: C 31.43, H 4.19, N 3.60, Re 48.47.

(4-Cyanopyridine)methyltrioxorhenium (1d): Yield: 330 mg (94 %); IR (KBr): $\tilde{\nu}$ = 1603 s (C=C), 1415 m, 1420 m, 943 vs (Re=O); 931 vs (Re=O), 842 s, 565 m cm^{-1}; ^{1}H NMR (400 MHz, $CDCl_3$, RT): δ = 2.15 ($ReCH_3$, s, 3H), 7.57 (N(CH)(C*H*), dd, ^{3}J(H,H) = 4.27 Hz, ^{4}J(H,H) = 1.22 Hz, 2H), 8.57 (N(C*H*), dd, ^{3}J(H,H) = 4.27 Hz, ^{4}J(H,H) = 1.22 Hz, 2H); ^{13}C{^{1}H} NMR (100.51 MHz, $CDCl_3$, RT): δ = 23.28 ($ReCH_3$), 115.76 (py-CN) 121.77 (N(CH)(*C*H)), 126.11 (N(CH)(CH)(*C*H)), 148.89 (N(CH)); CI-MS (70 eV): *m*/*z* (%): 251 (59) [CH_3ReO_3+H$^+$]$^+$, 235 (100) [ReO_3)]$^+$; anal. calcd for $C_7H_7N_2O_3Re$ (353.35): C 23.79, H 2.00, N 7.39, O 13.85, Re 52.70; found: C 23.79, H 2.01, N 8.01, O 13.51, Re 52.45.

Methyl(pyridine-4-aldehyde)trioxorhenium (1e): Yield: 250 mg (70 %); IR (KBr): $\tilde{\nu}$ = 1714 s (C = O), 1681 m (C=C), 1420 m, 1388 m, 939 vs (Re=O), 928 vs (Re=O), 821 s, 561 m, 478 m cm^{-1}; ^{1}H NMR (250 MHz, $CDCl_3$, RT): δ = 2.06 ($ReCH_3$, s, 3H), 7.73 (N(CH)(C*H*), dd, ^{3}J(H,H) = 4.75 Hz, ^{4}J(H,H) = 1.75 Hz, 2H), 8.51 (N(C*H*), dd, ^{3}J(H,H) = 4.50 Hz, ^{4}J(H,H) = 1.70 Hz, 2H); ^{13}C{^{1}H} NMR 62.90 MHz, $CDCl_3$, RT): δ = 23.80 ($ReCH_3$), 123.35 (N(CH)(*C*H)), 142.75 (N(CH)(CH)(*C*-C(O)H)), 148.83 (N(CH)), 190.40 (*C*HO); CI-MS (70 eV): *m*/*z* (%): 251 (100) [CH_3ReO_3+H]$^+$, 235 (78) [ReO_3)]$^+$; anal. calcd for $C_7H_8NO_4Re$ (356.35): C 23.59, H 2.26, N 3.93, O 17.96, Re 52.52; found: C 23.70, H 2.28, N 3.97, O 17.49, Re 52.35.

Methyl(pyrazole)trioxorhenium (1h): Yield: 298 mg (73 %). *Spectroscopic data:* IR (KBr): $\tilde{\nu}$ = 1528 m (C=C), 1471 m, 1405 m, 1358 w, 1278 w, 1259 m, 1190 w, 1161 w, 1122 m, 1058 m, 1046 m, 970 s (Re=O), 949 vs (Re=O), 879 w, 762 s, 709 s, 601 m, 525 m, 421 m cm^{-1}; ^{1}H NMR (400 MHz, $CDCl_3$, RT): δ = 2.18 ($ReCH_3$, s, 3H), 6.43 (N(H)(CH)(C*H*), d, 1H), 7.60 (N(H)(C*H*), d, 2H); ^{13}C{^{1}H} NMR (100.51 MHz, $CDCl_3$, RT): δ = 24.62 ($ReCH_3$), 134.22 (N(CH)(*C*H) and NH(*C*H)), 107.05 (N(H)(*C*H)),; CI-MS (70 eV): *m*/*z* (%): 251 (100) [CH_3ReO_3+H]$^+$, 235 (71) [ReO_3)]$^+$; anal. calcd for $C_4H_7N_2O_3Re$ (317.12): C 15.15, H 2.22, N 8.83; found: C 15.24, H 2.27, N 8.96.

Preparation of bis(methyltrioxorhenium)4,4′-bipyridine (1f) and bis-(methyltrioxorhenium)(1,2-bis(4-pyridyl)ethane) (1g): MTO (500 mg, 2 mmol) was dissolved in diethyl ether (10 mL) and 4,4′-bipyridine (4,4′-bis(methylenpyridine)) (1 mmol) was added to the stirred solution. The solution immediately turned yellow. After 1 h the solvent was evaporated in a vacuum (oil pump) and a pale yellow powder was obtained. This powder was washed with *n*-hexane (10 mL), the solution filtered off with a canula. The remaining yellow residue was dried in a vacuum (oil pump).

1f: Yield: 538 mg (82 %); IR (KBr): $\tilde{\nu}$ = 3090 w, 3057, m, 2987 w, 1604 s (C=C), 1413 s, 1384 m, 1218 m, 1074 m, 1005 m, 940 sst (Re=O), 928 vs (Re=O), 817 s, 626 m, 562 m, 489 w cm^{-1}; ^{1}H NMR (400 MHz, $CDCl_3$, RT): δ = 2.20 ($ReCH_3$, s, 6H), 7.56 (N(CH)(C*H*), dd, ^{3}J(H,H) = 4.52 Hz, 4H), 8.52 (N(C*H*), dd, ^{3}J(H,H) = 4.52 Hz, 4H); ^{13}C{^{1}H} NMR 62.90 MHz, $CDCl_3$, RT): δ = 23.26 ($ReCH_3$), 122.71 (N(CH)(*C*H)), 149.23 (N(CH)), 146.93 (N(CH)(CH)*C*); CI-MS (70 eV): *m*/*z* (%): 251 (100) [CH_3ReO_3+H]$^+$, 235 (67) [ReO_3)]$^+$; anal. calcd for $C_{12}H_{14}N_2O_6Re_2$ (654.67): C 22.02, H 2.16, N 4.28, Re 56.89; found: C 21.99, H 2.18, N 4.28, Re 56.95.

1g: Yield: 620 mg (90 %); IR (KBr): $\tilde{\nu}$ = 3092 w, 3050, m, 2976 m, 1946 s, 1610 (C=C), 1413 m, 1359 m, 1217 m, 1070 m, 1020 m, 939 sst (Re=O), 926 vs (Re=O), 827 s, 807 m, 739 m, 571 m, 546 m, 516 w, 495 w cm^{-1}; ^{1}H NMR (400 MHz, $CDCl_3$, RT): δ = 1.86 ($ReCH_3$, br., 6H), 7.09 (N(CH)(C*H*), br., 4H), 8.26 (N(C*H*), br., 4H),2.92 ((CH_2)$_2$, br., 4H); CI-MS (70 eV): *m*/*z* (%): 251 (100) [CH_3ReO_3+H]$^+$, 235 (71) [ReO_3)]$^+$; anal. found (calcd for $C_{14}H_{18}N_2O_6Re_2$ (682.72): C 24.63, H 2.66, N 4.10, Re 54.55; found: C 24.59, H 2.65, N 4.11, Re 54.51.

X-ray structure determination

General procedure: Suitable single crystals for the X-ray diffraction studies were grown by standard techniques from saturated solutions of **1c** in toluene and of **1f** in CH_2Cl_2/$(CH_3)_2O$/Et_2O at room temperature. Both structures were solved by a combination of Patterson syntheses and difference-Fourier syntheses and refined by full-matrix least-squares calculations. Neutral-atom scattering factors for all atoms and anomalous dispersion corrections for the non-hydrogen atoms were taken from the *International Tables for X-Ray Crystallography*.[34] All calculations were performed on a DEC station 5000/25 (**1c**) and a DEC 3000 AXP workstation (**1f**) with the STRUX-V system,[35] and used the programs PLATON,[36] SDP (**1c**),[37] SHELXS-86,[38] and SHELXL-93.[39] A summary of the crystal and experimental data is reported in Table 4.

(4-*tert*-Butylpyridine)methyltrioxorhenium (1c): Preliminary examination and data collection were carried out on an automated four-circle diffractometer (NONIUS CAD4) equipped with a sealed tube and graphite monochromated $Mo_{K\alpha}$ radiation. Final lattice parameters were obtained by least-squares refinement of 25 automatically centered high-angle reflections ($39.9° < 2\theta < 47.9°$). Data collection was performed at 193 K.[40] A total number of 4703 reflections were collected. Data were corrected for Lorentz and polarization effects. Corrections for absorption effects were applied (numerical, 8 indexed faces, T_{max}/T_{min}: 0.330/0.058). No decay was observed. After merging, a total of 2070 independent reflections remained which were used for all calculations. All "heavy atoms" of the asymmetric unit were anisotropically refined. All hydrogen atoms were placed in calculated positions and included in the structure factor calculations; however, they were not refined. The refinements was stopped at shift/err < 0.0001, and final difference Fourier maps showed no significant features. Full-matrix least-squares refinements were carried out by minimizing $\Sigma w(F_o^2 - F_c^2)^2$ with the SHELXL-93 weighting scheme.

Bis(methyltrioxorhenium)4,4′-bipyridine (1f): Preliminary examination and data collection were carried out on a Kappa CCD area detecting

Table 4. Crystallographic data for [(4-*tert*-butylpyridine)(CH_3)ReO_3] (**1c**), and [4,4′-bipy{(CH_3)ReO_3}$_2$] (**1f**)

	1c	**1f**
formula	$C_{10}H_{16}NO_3Re$	$C_{12}H_{14}N_2O_6Re_2$
Fw	384.45	654.67
color/habit	yellow/plate	colorless/plate
cryst. size [mm]	$0.36 \times 0.11 \times 0.056$	$0.45 \times 0.35 \times 0.08$
cryst. system	orthorhombic	monoclinic
space group	*Pbcn*	$P2_1/n$
a [Å]	16.720(1)	6.3455(3)
b [Å]	8.345(1)	5.2880(1)
c [Å]	17.981(1)	24.1601(12)
β [°]		97.387(1)
V [Å^3]	2508.9(4)	803.96(6)
Z	8	2
ρ_{calcd} [g cm^{-3}]	2.036	2.704
F_{000}	1456	596
λ [Å]	0.71073	0.71073
μ [mm^{-1}]	9.68	15.07
device/scan method	CAD 4/ω scan	Kappa CCD/–
Θ range [°]	2.27 to 24.97	3.24 to 26.36
data collcd [*h*,*k*,*l*]	+19, +9, +21	±7, ±4, ±30
no. of reflections collected	4703	5599
no. of independent reflections	2070	1391
no. of observed reflections	2070 (all data)	1391 (all data)
no. of parameters refined	136	100
R_{int}	0.015	0.0428
*R*1[a]	0.0349	0.0428
*wR*2[b]	0.0733	0.1190
GOF[c]	1.100	1.147
weights a/b[d]	0.0459/0	0.0790/1.4121
$\Delta\rho_{max/min}$ [e Å^{-3}]	0.96/−1.39	+0.98/−2.51[e]

[a] $R1 = \Sigma(||F_o| - |F_c||)/\Sigma|F_o|$. [b] $wR2 = [\Sigma w(F_o^2 - F_c^2)^2/\Sigma w(F_o^2)^2]^{1/2}$; [c] $GOF = [\Sigma w(F_o^2 - F_c^2)^2/(NO\text{-}NV)]^{1/2}$; [d] $w \equiv 1/[\sigma^2(F_o^2) + (a*P)^2 + b*P]$ with P: [max (0 or F_o^2) + $2F_c^2$]/3. [e] The remarkably high negative value is caused by an unsatisfactory correction for absorption effects.

diffraction system (NONIUS; MACH 3) equipped with a rotating anode and graphite-monochromated $Mo_{K\alpha}$ radiation. The unit cell parameters were obtained by full-matrix least-squares refinements of 6311 reflections. Data collection was performed at 293 K (exposure time: 120 s per frame; θ-offset: 10°, φ: 0.0°–360.0°; $\Delta\varphi$:1°; dx: 40.0 mm). A total number of 5599 reflections were collected. Raw data were reduced and scaled with the programs DENZO and HKL.[41, 42] Data were corrected for Lorentz and polarization effects. Corrections for absorption effects were applied with the difabs strategy (T_{max}/T_{min}: 1.000/0.130).[36] After merging, a total of 1391 independent reflections remained which were used for all calculations. All "heavy atoms" of the asymmetric unit were refined anisotropically. All hydrogen atoms were placed in calculated positions and included in the structure factor calculations; however, they were not refined. Full-matrix least-squares refinements were carried out by minimizing $\Sigma w(F_o^2 - F_c^2)^2$ with the SHELXL-93 weighting scheme and stopped at shift/err < 0.001.

Crystallographic data (excluding structure factors) for the structures reported in this work have been deposited with the Cambridge Crystallographic Data Centre as supplementary publication nos. CCDC-116367 (**1c**) and CCDC-116366 (**1f**). Copies of the data can be obtained free of charge on application to CCDC, 12 Union Road, Cambridge CB2 1EZ, UK (fax: (+44) 1223-336-033; e-mail: deposit@ccdc.cam.ac.uk).

Catalysis: Catalytic reactions with compounds **1x** as catalysts:

Method A: *cis*-Cyclooctene (800 mg, 7.3 mmol) and *n*-dibutylether (800 mg, internal standard), with **1** (1 mol%, 73 μmol) as the catalyst. The amount of ligand changed from 73 μmol (1:1) to 1.8 mmol (1:25)

b) *Method B*: Styrene (200 mg, 1.7 mmol) and mesitylene (100 mg, 0.83 mmol, internal standard), with **1** (1 mol%, 17 μmol) as the catalyst. The amount of ligand changed from 17 μmol (1:1) to 0.17 mmol (1:10)

For both Method A and B, hydrogen peroxide (1.5 mL, 35%) was added to a thermostated reaction vessel and stirred for 4 h at 25 °C. In the catalytic runs conducted at 55 °C toluene was used as the solvent. The course of the reaction was monitored by quantitative GC analysis; samples were taken every 10 min, diluted with methylene chloride, and chilled in an ice bath. For the destruction of the hydrogen peroxide and removal of water, a catalytic amount of manganese dioxide and magnesium sulfate was added. After the evolution of gas ceased, the resulting slurry was filtered over a filter equipped with a Pasteur pipette and the filtrate injected into a GC column. The conversion of cyclooctene and styrene, respectively, and the formation of cyclooctene oxide and styrene oxide was calculated from a calibration curve ($r^2 = 0.999$) recorded prior to the reaction course.

Computational procedures: All the electronic structure calculations were performed with the hybrid B3-LYP[43] density functional scheme[44] with effective core potentials.[45] Geometry optimizations were carried out without any symmetry restrictions with 6-311G(d,p)[46] on all centers (except Re). Finally, two *f* exponents were added to the basis set of Re to evaluate energies in a single-point fashion.[5] Details of this computational strategy have been discussed elsewhere.[47] Since the present study focuses on trends and their explanation, we refrained from correcting stabilization energies and reaction barriers for enthalpy and solvent effects. Previous investigations have shown that such corrections do not affect the trends analyzed in the present study.[5, 47]

Acknowledgments

The authors are grateful to Prof. Dr. W. A. Herrmann for his continuous support. A.M.S. thanks the Bayerische Forschungstiftung for a fellowship. The work was also supported by the Deutsche Forschungsgemeinschaft (DFG), the Bayerischer Forschungsverbund Katalyse (FORKAT), the German Bundesministerium für Bildung, Wissenschaft, Forschung und Technologie (grant no. 03D0050B), and the Fonds der Chemischen Industrie.

[1] R. Jira, R. A. Sheldon in *Applied Homogeneous Catalysis with Organometallic Compounds*, *Vol. 1*, (Eds.: B. Cornils, W. A. Herrmann), Wiley-VCH, Weinheim, **1996**, 374.
[2] W. A. Herrmann, R. W. Fischer, D. W. Marz, *Angew. Chem.* **1991**, *103*, 1706; *Angew. Chem. Int. Ed. Engl.* **1991**, *30*, 1638.
[3] W. A. Herrmann, R. W. Fischer, W. Scherer, M. U. Rauch, *Angew. Chem.* **1993**, *105*, 1209; *Angew. Chem. Int. Ed. Engl.* **1993**, *32*, 1157.
[4] For a recent review, see for example: W. A. Herrmann, F. E. Kühn, G. M. Lobmaier in *Aqueous-Phase Organometallic Catalysis: Concepts and Applications* (Eds: B. Cornils, W. A. Herrmann), Wiley-VCH, Weinheim, **1998**, 529.
[5] P. Gisdakis, S. Antonczak, S. Köstlmeier, W. A. Herrmann, N. Rösch, *Angew. Chem.* **1998**, *110*, 2331; *Angew. Chem. Int. Ed.* **1998**, *37*, 2211.
[6] W. A. Herrmann, R. W. Fischer, M. U. Rauch, W. Scherer, *J. Mol. Catal.* **1994**, *86*, 243.
[7] W. Adam, C. M. Mitchel, *Angew. Chem.* **1996**, *108*, 578; *Angew. Chem. Int. Ed. Engl.* **1996**, *35*, 533.
[8] T. R. Boehlow, C. D. Spilling, *Tetrahedron Lett.* **1996**, *37*, 2717.
[9] W. A. Herrmann, F. E. Kühn, M. R. Mattner, G. R. J. Artus, M. R. Geisberger, J. D. G. Correia, *J. Organomet. Chem.* **1997**, *538*, 203.
[10] J. Rudolph, K. L. Reddy, J. P. Chiang, K. B. Sharpless, *J. Am. Chem. Soc.* **1997**, *119*, 6189.
[11] A. K. Yudin, K. B. Sharpless, *J. Am. Chem. Soc.* **1997**, *119*, 11536.
[12] C. Copéret, H. Adolfsson, K. B. Sharpless, *J. Chem. Soc. Chem. Commun.* **1997**, 1915.
[13] W. A. Herrmann, R. M. Kratzer, H. Ding, H. Glas, W. R. Thiel, *J. Organomet. Chem.* **1998**, *555*, 293.
[14] W. A. Herrmann, H. Ding, R. M. Kratzer, F. E. Kühn, J. J. Haider, R. W. Fischer, *J. Organomet. Chem.* **1997**, *549*, 319.
[15] W. A. Herrmann, J. D. G. Correia, M. U. Rauch, G. R. J. Artus, F. E. Kühn, *J. Organomet. Chem.* **1997**, *118*, 33.
[16] W. D. Wang, J. H. Espenson, *J. Am. Chem. Soc.* **1998**, *120*, 11335.
[17] a) S. Köstlmeier, O. D. Häberlen, N. Rösch, W. A. Herrmann, B. Solouki, H. Bock, *Organometallics*, **1996**, *15*, 1872; b) S. Köstlmeier, V. A. Nasluzov, W. A. Herrmann, N. Rösch, *Organometallics* **1997**, *16*, 1786.

 © WILEY-VCH Verlag GmbH, D-69451 Weinheim, 1999 0947-6539/99/0512-3614 $ 17.50+.50/0

[18] W. A. Herrmann, J. G. Kuchler, G. Weichselbaumer, E. Herdtweck, P. Kiprof, *J. Organomet. Chem.* **1989**, *372*, 351.
[19] W. A. Herrmann, G. Weichselbaumer, E. Herdtweck *J. Organomet. Chem.* **1989**, *372*, 371.
[20] W. A. Herrmann, F. E. Kühn, M. U. Rauch, J. D. G. Correia, G. R. J. Artus, *Inorg. Chem.* **1995**, *34*, 2914.
[21] M. H. P. Rietveld, L. Nagelholt, D. M. Grove, N. Veldman, A. L. Spek, M. U. Rauch, W. A. Herrmann, G. van Koten, *J. Organomet. Chem.* **1997**, *530*, 159.
[22] W. A. Herrmann, R. W. Fischer, W. Scherer, *Adv. Mater.* **1992**, *4*, 653.
[23] H. Rudler, J. R. Gregorio, B. Denise, J. M. Brégeault, A. Deloffre, *J. Mol. Catal.* **1998**, *133*, 255.
[24] W. A. Herrmann, F. E. Kühn, C. C. Romão, *J. Organomet. Chem.* **1995**, *489*, C56.
[25] *The Chemistry of Heterocyclic Compounds*, *Pyridine and its Derivatives*, Part I, Chapt. I and Part II, Chapt. 5, Interscience Publishers, New York, USA, **1960**.
[26] C. C. Romão, F. E. Kühn, W. A. Herrmann, *Chem. Rev.* **1997**, *97*, 3197.
[27] J. Mink, G. Keresztury, A. Stirling, W. A. Herrmann, *Spectrosc. Chim. Acta* **1994**, *50A*, 2039.
[28] C. Mealli, J. A. Lopez, M. J. Calhorda, C. C. Romão, W. A. Herrmann, *Inorg. Chem.* **1994**, *33*, 1139.
[29] M. M. Abu-Omar, P. J. Hansen, J. H. Espenson, *J. Am. Chem. Soc.* **1996**, *118*, 4966.
[30] W. Adam, D. Golsch, J. Sundermeyer, G. Wahl, *Chem. Ber.* **1996**, *129*, 1177.
[31] C. Di Valentin, P. Gisdakis, I. V. Yudanov, N. Rösch, unpublished results.
[32] a) D. A. Singleton, S. R. Merrigan, J. Liu, K. N. Houk, *J. Am. Chem. Soc.* **1997**, *119*, 3385; b) R. D. Bach, C. M. Estévez, J. E. Winter, M. N. Glukhovtsev, *J. Am. Chem. Soc.* **1998**, *120*, 680.
[33] W. A. Herrmann, F. E. Kühn, R. W. Fischer, W. R. Thiel, C. C. Romão, *Inorg. Chem.* **1992**, *31*, 4431.
[34] *International Tables for Crystallography*, *Vol. C*, Tables 6.1.1.4 (pp. 500–502), 4.2.6.8 (pp. 219–222), and 4.2.4.2 (pp. 193–199), (Ed.: A. J. C. Wilson), Kluwer, Dordrecht (The Netherlands), **1992**.
[35] G. Artus, W. Scherer, T. Priermeier, E. Herdtweck, STRUX-V, A Program System to Handle X-ray Data, TU München (Germany), **1997**.
[36] A. L. Spek, PLATON - PLUTON, An Integrated Tool for the Analysis of the Results of a Single Crystal Structure Determination, *Acta Crystallogr. Sect. A* **1990**, *46*, C34.
[37] B. A. Frenz, "Enraf-Nonius SDP-Plus Structure Determination Package". Version 4.0. Enraf-Nonius, Delft (The Netherlands), **1988**.
[38] G. M. Sheldrick, SHELXS-86, A Program for the Solution of Crystal Structures from Diffraction Data, *Acta Crystallogr. Sect. A* **1990**, *46* , 467.
[39] G. M. Sheldrick, SHELXL-93, in *Crystallographic Computing 3*, (Eds.: G. M. Sheldrick, C. Krüger, R. Goddard), Oxford University Press, **1993**, pp. 175
[40] L. Straver, "Enraf-Nonius CAD 4 Operating System" Version 5.0, B. V. Enraf-Nonius, Delft (The Netherlands), **1989**.
[41] Data Collection Software for Nonius Kappa CCD, Delft (The Netherlands), **1997**.
[42] Z. Otwinowski, W. Minor, "Processing of X-ray Diffraction Data Collected in Oscillation Mode", *Methods in Enzymology 276*, (Eds.: W. C. Carter, R. M. Sweet, Jr.), Academic Press (USA), **1996**.
[43] a) A. D. Becke, *J. Chem. Phys.* **1993**, *98*, 5648; b) C. Lee, W. Yang, R. G. Parr, *Phys. Rev. B* **1988**, *37*, 785.
[44] M. J. Frisch, G. W. Trucks, H. B. Schlegel, P. M. W. Gill, B. G. Johnson, M. A. Robb, J. R. Cheeseman, T. Keith, G. A. Petersson, J. A. Montgomery, K. Raghavachari, M. A. Al-Laham, V. G. Zakrzewski, J. V. Ortiz, J. B. Foresman, J. Cioslowski, B. B. Stefanov, A. Nanayakkara, M. Challacombe, C. Y. Peng, P. Y. Ayala, W. Chen, M. W. Wong, J. L. Andres, E. S. Replogle, R. Gomperts, R. L. Martin, D. J. Fox, J. S. Binkley, D. J. Defrees, J. Baker, J. P. Stewart, M. Head-Gordon, C. Gonzalez, and J. A. Pople, GAUSSIAN 94, Revision D.4, Gaussian, Inc., Pittsburgh PA, USA, **1995**.
[45] a) P. J. Hay, W. R. Wadt, *J. Chem. Phys.* **1985**, *82*, 299; b) G. Frenking, I. Antes, M. Böhme, S. Dapprich, A. W. Ehlers, V. Jonas, A. Neuhaus, M. Otto, R. Stegmann, A. Veldkamp, S. F. Vyboishchikov in *Reviews in Computational Chemistry*, *Vol. 8* (Eds.: K. B. Lipkowitz, D. B. Boyd), VCH, New York, **1996**, p. 63.
[46] R. Krishnan, J. Binkley, R. Seeger, J. Pople, *J. Chem. Phys.* **1980**, *72*, 650.
[47] P. Gisdakis, S. Antonczak, N. Rösch, *Organometallics* in press.

Received: March 16, 1999 [F 1679]